GEOPHYSICS, VOL. 71, NO. 4 (JULY-AUGUST 2006); P. SI79–SI84, 8 FIGS.
10.1190/1.2215360

On estimating the impulse response between receivers in a controlled ultrasonic experiment

K. van Wijk[1]

ABSTRACT

A controlled ultrasonic laboratory experiment provides a detailed analysis of retrieving a band-limited estimate of the Green's function between receivers in an elastic medium. Instead of producing a formal derivation, this paper appeals to a series of intuitive operations, common to geophysical data processing, to understand the practicality of seismic interferometry. Whereas the retrieval of the full Green's function is based on the crosscorrelation of receivers in the presence of equipartitioned signal, an estimate of the impulse response is recovered successfully with 40 sources in a line covering six wavelengths at the surface.

INTRODUCTION

Crosscorrelating an arbitrary input of a linear system with the resulting output is the basic idea behind the matched filter. As early as 1950, it was known that this crosscorrelation would synthesize the impulse response of a linear system (Lee, 1960), using a random signal as an input. Matched filtering later found its way into geophysics, most prominently in processing vibroseis data. More recently, derivations of the emergence of the Green's function between receivers surfaced. Closely related to matched filtering, arguments of stationary phase (Snieder, 2004), time-reversal (Derode et al., 2003), and normal-mode expansions (Lobkis and Weaver, 2001; Weaver and Lobkis, 2001) have led to the same conclusion that the impulse response between any two receivers can be obtained from the crosscorrelation of the recorded wavefields.

Accurate estimates of the impulse response between any two receivers is potentially significant in seismology. While earthquake sources are limited mostly to plate boundaries, seismic interferometry could provide sources at each seismic recording station. In addition, at the exploration scale, one could increase stacking fold cheaply while avoiding sources in sensitive areas where dynamite and vibroseis are not appropriate. In time-lapse experiments, source repeatability is a problem, but in seismic interferometry, knowing receiver locations is sufficient. For a full Green's function retrieval, the equipartition of waves is necessary. Equipartition means that all directions of propagation are equally likely; i.e., the wavefield has no preferred wavenumber. This can be achieved in two ways. First, an impulsive source scatters in a heterogeneous medium enough times so that at late times (coda), equal energy is propagating in all directions (Malcolm et al., 2004). Second, one can imagine a scenario in which a (random) distribution of sources directly creates equipartitioned energy. The latter has been labeled *ambient noise*, but is more a case of unexplained signal: Actual coherent waves — no matter how weak — have to propagate between the receivers to retrieve the Green's function in a heterogeneous medium.

In geophysics, acoustic waves inside the sun have been synthesized from random fluctuations at the sun's surface (Duvall et al., 1993; Rickett and Claerbout, 1999). Studies in seismic coda and passive recordings of natural sources have focused on the retrieval of the surface-wave Green's function in the earth (Campillo and Paul, 2003; Shapiro and Campillo, 2004; Sabra et al., 2005; Shapiro et al., 2005). This could have a number of reasons. First, the responses of these unknown sources could be dominated by surface waves. Second, geometrical spreading of surface waves is limited to two dimensions. Because geometrical spreading of body waves is 3D, at late times, seismic energy is dominated by surface waves. Finally — if scattering is not strong enough to distribute energy throughout the earth, and if our sources (earthquakes, water waves, human noise, microseismicity) are limited in space and time — body waves might not be present (or attenuated) in the data used for seismic interferometry. This can be side-stepped using active seismic sources (Bakulin and Calvert, 2004; Schuster et al., 2004).

Experiments on an ultrasonic laboratory model introduce established — and investigate outstanding — issues in seismic interferometry through a series of intuitive steps towards the band-limited Green's function retrieval between receivers. Even in the case of limited sources on the surface only (and hence limited energy coverage of the subsurface), I obtain accurate estimates of the vertical

Manuscript received by the Editor June 15, 2005; revised manuscript received December 22, 2005; published online August 17, 2006.
[1]Physical Acoustics Laboratory and Department of Geophysics, Colorado School of Mines, 1500 Illinois Street, Golden, Colorado 80401. Email: kasper@acoustics.mines.edu.

component of the band-limited impulse response in a homogeneous slab of granite. The next section explains the basic experimental setup and provides an estimate of the impulse response from a single measurement with one source and one receiver, which will be compared to estimates of the Green's function between receivers in further sections. First, the crosscorrelation between two receivers for a single source is linked to matched filtering, then the discussion is expanded to experiments with multiple-source positions, and more than two receivers.

A DIRECT ESTIMATE OF THE IMPULSE RESPONSE

The centers of two piezoelectric *P*-wave transducers (2.54-cm diameter) are separated by 100 mm atop a slab of granite (x = y = 620 × z = 105 mm^3). A side view of the experimental geometry is shown in the top panel of Figure 1. The *P*-wave speed in the granite is estimated to be 6300 m/s; the *S*-wave speed 3300 m/s, and the Rayleigh wave speed 3150 m/s. The source is driven by a 200-V pulse, exciting an impulsive ultrasonic source function $S(x',t)$ that emits *P*-wave, surface-wave, and a small amount of *S*-wave energy. The dominant *P* wavelength in the granite is between 25 and 30 mm. This is more than ten times the average grain size in the granite, so scattering from the individual grains can be neglected. This means that the medium is homogeneous for all practical purposes. The vertical component of the particle acceleration, recorded 10 cm from the source consisting of direct waves and scatterings from the boundaries of the slab, is

$$u(x, t) = G(x', x, t) \otimes S(x', t), \tag{1}$$

where $G(x', x, t)$ is the Green's function — or impulse response — for the vertical component of the particle acceleration in the granite slab between source $S(x', t)$ at horizontal location x' and the receiver at the surface with horizontal position x, while $\otimes$ denotes convolution. Coherent events in $u(x, t)$ annotated in the bottom panel of Figure 1 include the direct *P*-wave, the direct Rayleigh wave, the *P*-wave reflection from the bottom (*PP*) and its multiples (*PPPP*, *PPPPPP*), as well as a wave mode, converted at the bottom of the slab (*PS*) and its multiple (*PSPP*). The recording time is limited such that signals from the sides of the granite out-of-plane does not reach the detector.

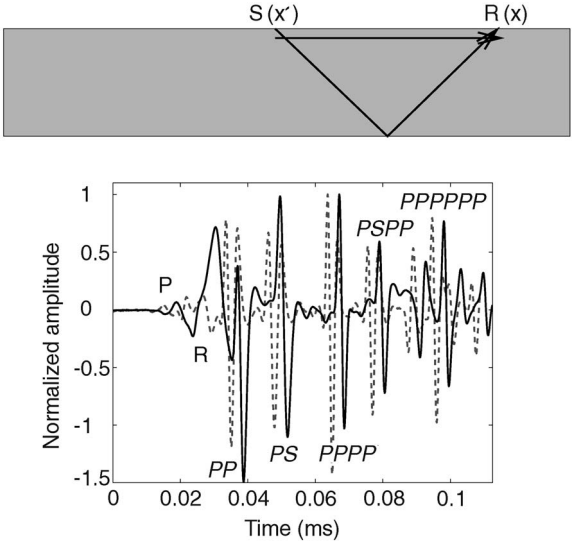

Figure 1. Top: Side view of a source and receiver separated by 10 cm on a granite slab (x = y = 620 × z = 105 mm^3), with paths for the direct-surface wave and one reflected wave. These waves, plus multiple reflections and mode conversions, are present in the unfiltered [$u(x, t)$, solid line] and the phase-shifted, filtered [$\widetilde{G}(x', x, t)$, dashed line] wavefields (bottom).

The solid line in Figure 1 is the unprocessed recording $u(x, t)$. The dashed line is the zero-phase and bandpass-filtered (50-kHz–1-MHz) version of $u(x, t)$. Figure 2 illustrates the applied phase shift via a zoom of the *PPPP* arrival: The causal wavelet (solid line) is shifted to a(n almost) zero-phase wavelet (dashed line). In the filtering process, a large amount of the surface-wave energy in $S(t)$ is lost, but the goal of this processing step is to find the zero-phase source function $\widetilde{S}(t)$. This way, the processed version of the waveform $u(x, t)$ is

$$G(x', x, t) \otimes \widetilde{S}(x', t) = \widetilde{G}(x', x, t). \tag{2}$$

$\widetilde{G}(x', x, t)$ is a band-limited version of the true Green's function $G(x', x, t)$. All further recordings undergo this bandpass filter and phase shift, minimizing the influence of the original source function $S(t)$.

CROSSCORRELATING TWO RECEIVERS FROM A SINGLE SOURCE

From here on, the purpose is to retrieve information about the impulse response for the vertical component of the particle acceleration between receivers. This sequence of experiments is to illustrate that important information between receivers can be obtained with just a few sources in a limited region, using some basic techniques commonly applied in geophysical data processing. First, the source from the previous section is replaced by a receiver at x'. The new source is placed approximately 10 cm to the left of the receivers at position x^s. Both receivers recorded 2250 samples at 10^7 samples per second of the vertical component of the particle acceleration. The crosscorrelation between the phase-shifted and filtered waveforms is

$$C^s(t) = \widetilde{G}(x^s, x', t) \star \widetilde{G}(x^s, x, t), \tag{3}$$

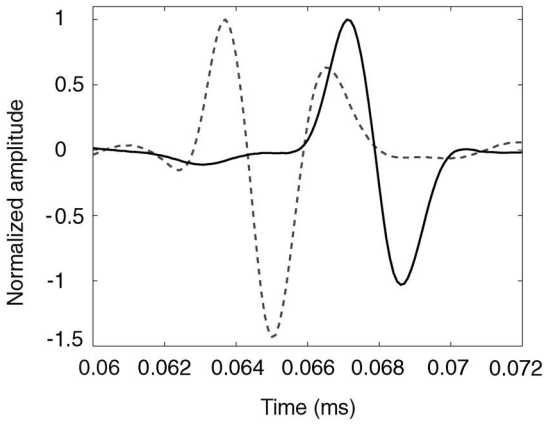

Figure 2. A zoom of the *PPPP* event of $u(x, t)$ (solid line) and $\widetilde{G}(x', x, t)$ (dashed line).

where ⋆ denotes crosscorrelation. $C^s(t)$ includes the autocorrelation of the source function, which is by definition zero-phase, just as the source in $\widetilde{G}(x', x, t)$.

The bottom panel of Figure 3 compares the crosscorrelation of the two wavefields $C^s(t)$ (solid line) and $\widetilde{G}(x', x, t)$ (dashed line). In this figure, and for all crosscorrelations in further figures, amplitudes are normalized to one. With the source to the left of x', $C^s(t)$ contains strong correlations for waves that first visit the receiver at x' and, then, the receiver at x. This can be seen as an example of Huygens' principle: The wavefield at x' acts as a secondary source for the wavefield recorded at x. These paths are the solid lines in the top panel of Figure 3 and are part of $\widetilde{G}(x', x, t)$. For these waves, equation 3 represents a matched filter: If the source position coincides with either of the receiver locations, all waves go through both receivers. However, correlations in $C^s(t)$ also occur when coherent events arrive that do not intersect both receivers. An example of these is the correlation between the dashed line and any of the solid-line arrivals in the top panel of Figure 3. Such correlations lead to the peaks in $C^s(t)$ before $t = 0.03$ ms. Not only is there a correlation in $C^s(t)$ between the single-bounce reflection to both receivers: In the presence of many wave modes (*P*- and *S*-wave reflections, converted and surface waves), correlations occur between waves of different modes. One way of minimizing the correlations between different wave modes is to split the recordings of the different modes in the medium, and crosscorrelate recordings of each mode separately (Wapenaar, 2004).

A normalized correlation coefficient is computed to quantify the match between $C^s(t)$ and $\widetilde{G}(x', x, t)$. For identical waveforms, this correlation is unity. Here, the correlation between the two waveforms is 0.65. Even though the bottom panel of Figure 3 shows that $C^s(t)$ contains some resemblance to the direct measurement of the Green function $\widetilde{G}(x', x, t)$, the next section improves our estimate of $\widetilde{G}(x', x, t)$ from crosscorrelating receivers by minimizing the correlations between waves that do not go through both receivers.

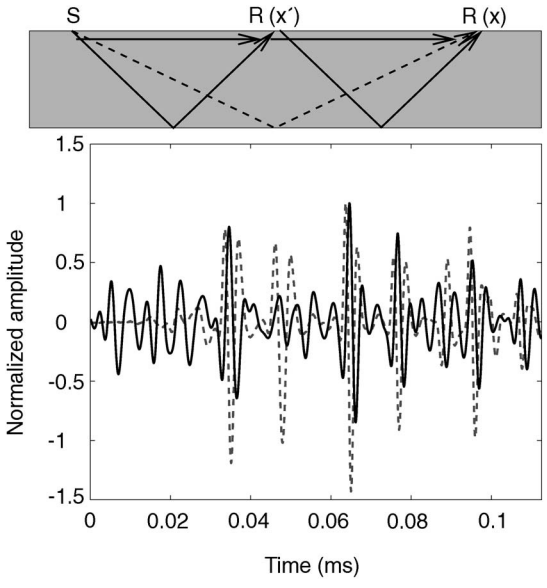

Figure 3. Top: Side view of the granite slab. Waves that go through both receivers (solid lines) crosscorrelate in a way that agrees with $\widetilde{G}(x', x, t)$. Correlation between waves with a solid and a dashed path are not present in $\widetilde{G}(x', x, t)$. Bottom: Comparison between $\widetilde{G}(x', x, t)$ (dashed, same as dashed line in Figure 1) and the crosscorrelation of the recorded wavefields from one source ($C^s(t)$, solid).

CROSSCORRELATING TWO RECEIVERS, SUMMING OVER SOURCES

Imagine we had not one, but a number of sources, in different locations. This situation can be obtained from a single source in a strongly scattering medium via Huygens' principle or from active sources in a homogeneous medium. (In practice, there will likely be a combination of these two scenarios.) In either case, we can compute the summed crosscorrelation between receivers:

$$\underline{C}(t) = \sum_{s=1}^{N} C^s(t) = \sum_{s=1}^{N} \widetilde{G}(x^s, x', t) \star \widetilde{G}(x^s, x, t), \qquad (4)$$

where N is the number of sources (active ones, or secondary Huygens sources) and $C^s(t)$ is the crosscorrelation for the sth source as defined in equation 3. Why would this be a better estimate of the band-limited impulse response $\widetilde{G}(x', x, t)$ than expression 3? The answer lies in the argument of stationary phase: The phase difference between events that arrive at the receivers, which did not pass through both receivers, differs for each source position. On the other hand, when a wave goes through both receivers, the phase difference in the arrival between them is constant, independent of the source position. Averaging over enough sources (source locations) suppresses the correlations between waves that do not intersect both receivers.

In this case, source locations are limited to the boundaries of the sample. To mimic a (scaled version of a) reflection seismic survey, sources are further limited to only the top of the granite slab. The top panel of Figure 4 shows the experimental configuration of $N = 40$ shots, spaced over $\sim$ 6 wavelengths (16 cm) to the left of x'. The data acquisition geometry is 2D along the line through the source and receivers. However, because the source radiation pattern is 3D,

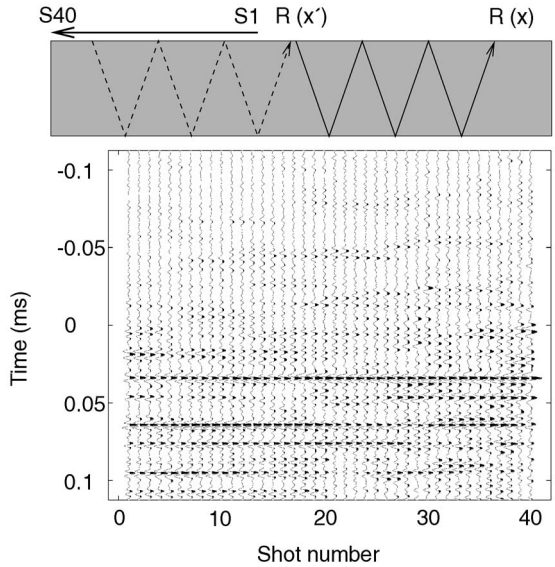

Figure 4. Top: Experimental geometry for 40 sources to the left of x'. Bottom: The crosscorrelation between receivers for each source. Stationary phase points are only for positive lags, relating to waves propagating from x' to x.

one could consider this experiment 2.5D. Again, the recording is terminated before the signal can reflect from the sides of the model away from the source-receiver line and return to the receiver. In addition, the same filtering and phase-shifting of $u(x, t)$ is applied to all recordings in this experiment.

The bottom panel of Figure 4 shows $C^s(t)$ for each source. Stationary phase points for positive time lags correspond to coherent waves traveling from x' to x [the causal part of $\widetilde{G}(x', x, t)$], while negative time lags relate to waves traveling from x to x' (anticausal part of $\widetilde{G}(x', x, t)$). There is no evidence of stationary phase points for waves from x to x'. This should not come as a surprise, because all sources are to the left of x'! On the other hand, all stationary phases for positive time lags can be related to the coherent events in Figure 1. While the stationary phase for the surface wave (at $t \approx 0.04$ ms) remains strong for sources as far as 6 wavelengths, the stationary phase for the *PPPPPP* event at $t \approx 0.09$ ms becomes less pronounced for sources further away from the receivers. The path for this event is sketched in the top panel of Figure 4. For source number 21 and higher (three wavelengths and more from x'), the wave from the source to the detector via 12 that bounces from the bottom of the slab, is not detected. Even in this medium with high Q, losses at the reflection points and geometric spreading complicate body-wave retrieval for our estimate of the Green's function. In addition, the *PS* event at $t \approx 0.05$ ms does not become a strong stationary phase point until source number 27, where the critical angle for *P-S* conversion is reached.

Stacking the bottom panel of Figure 4 leads to $\underline{C}(t)$. The solid line in Figure 5 is the causal part (waves from x' to x) of $\underline{C}(t)$. The maximum correlation factor between $\widetilde{G}(x', x, t)$ and $\underline{C}(t)$ is 0.76 but would require a negative time shift in $\underline{C}(t)$. Correlation around 0.01 ms in $C^s(t)$ (Figure 3), between waves that do not intersect both receivers correctly, cancels in $\underline{C}(t)$. The remaining discrepancy between $G(x', x, t)$ and $\underline{C}(t)$ is a phase difference, which is addressed in the following section.

TAKING A TIME DERIVATIVE

The time derivative of the crosscorrelation of receivers is necessary to obtain the Green's function in the presence of equipartitioned signal (Weaver and Lobkis, 2001; Snieder, 2004; Roux et al., 2005). Intuitively, this can be explained following Roux et al. (2005). Consider an impulsive surface-wave source recorded at x' (left) and x (right). For any source, the crosscorrelation of the receivers represents the time difference between the source traveling from x' and x. All sources to the left of receiver x' have a lag for the peak in the crosscorrelation equal to $t_{\max}$, the time for the surface wave to pass x' and to arrive at x. Conversely, the crosscorrelation of the receivers for sources to the right of x peak at $-t_{\max}$. Sources between the two receivers have lags as small as $t = 0$ for the source halfway between the receivers. When summing over all possible source positions, the peaks in the crosscorrelation of the receivers form a boxcar function between $-t_{\max}$ and $t_{\max}$. The time derivative of this boxcar function is the sum of the Dirac delta functions $\delta(t - t_{\max})$ and $-\delta(t + t_{\max})$, corresponding to the causal and anticausal Green's function for the direct-surface wave. The same argumentation holds for body-wave sources and zero-phase band-limited signal, as in our case.

The time derivative of the sum of receiver crosscorrelations over N sources is

$$\dot{\underline{C}}(t) = \frac{d}{dt}\left(\sum_{s=1}^{N} \widetilde{G}(x^s, x', t) \star \widetilde{G}(x^s, x, t) \right). \qquad (5)$$

The correlation between the resulting $\dot{\underline{C}}(t)$ and $\widetilde{G}(x', x, t)$ is 0.87 (Figure 6). If we consider a wavefield $\propto \exp(i\omega t)$, then its derivative is $\propto i\omega \exp(i\omega t)$, and it introduces a phase shift of i, or $\pi/2$ with respect to the original wavefield. Similarly, differentiation effectively dampens low-frequency variations, because of the extra frequency factor of ω in the derivative. The main remaining discrepancies between the two waveforms are lower amplitudes of the *PS* and *PPPPPP* event in $\dot{\underline{C}}(t)$. These are the same events discussed earlier as not having stationary phase points for all sources.

Whether $\dot{\underline{C}}(t)$ is a better estimate of the Green's function than $\underline{C}(t)$, is dependent on many factors. One is the nature of the source function and whether we measure particle acceleration, velocity, or displacement. Another factor is whether our signal is equipartitioned. For a theoretical discussion, please see Wapenaar and Fokkema (2006).

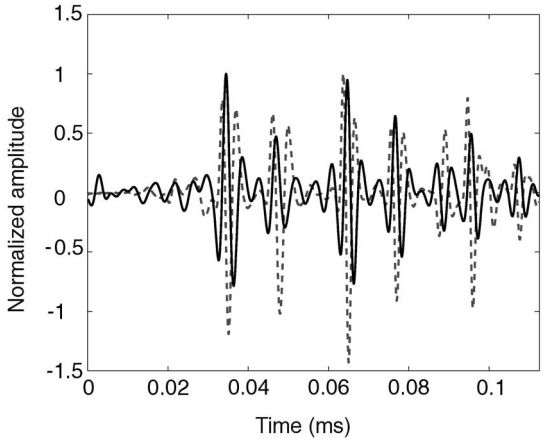

Figure 5. Comparison between $\widetilde{G}(x', x, t)$ (dashed line, same as Figure 1) and the summed crosscorrelation of the recorded wavefields for 40 source positions ($\underline{C}(t)$, solid line). The maximum correlation between the two waveforms is 0.76.

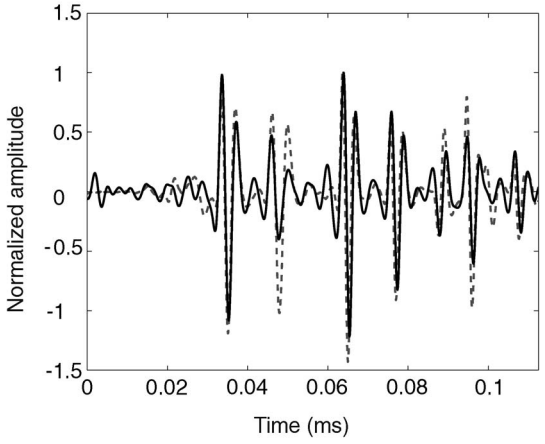

Figure 6. Comparison between $\dot{\underline{C}}(t)$ (solid line) and $\widetilde{G}(x', x, t)$ (dashed line, same as Figure 1). The correlation coefficient between these waveforms is 0.87.

A VIRTUAL SHOT RECORD

If spurious events remaining in $\dot{\underline{C}}(t)$ are spatially uncorrelated for different receiver pairs, $\dot{\underline{C}}(t)$ for an array of receivers is straightforward to decipher. This is illustrated by Figure 7: Instead of having two receivers, a laser vibrometer (Nishizawa et al., 1997; Scales and van Wijk, 1999) records the wavefield for 21 receiver locations over the same 10-cm line for the same 40 sources over a 16-cm line (top panel of Figure 7). The shaded plot in the bottom panel is a shot record for one source 35 mm from the first receiver, while the wiggles are the derivative of the summed crosscorrelations with respect to the first receiver. Events from direct surface waves to (multiple) reflections of *P*-waves and converted waves are coherent in both the shot record and the virtual shot record (wiggles). For source-detector offsets where the two records overlap (35–100 mm), the visual agreement is striking. Note that the shot and virtual shot records do not physically overlap for these offsets (see wave paths in the top panel of Figure 7), but for laterally homogeneous media, the waveforms agree. The result of Figure 7 is that the crosscorrelation of receivers has increased the range of (virtual) source-receiver offsets, and improved stacking power for overlapping source-detector offsets.

WHEN SOURCES OVERLAP IN TIME

In passive imaging, where the responses of seismic sources overlap in time — such as water waves crashing on shore or microseismic activity — the signal from each individual source cannot be separated. This stands in stark contrast to the earlier situation where the crosscorrelation of receivers is computed for each source individually, then summed and differentiated. This way, there are no correlations between events from different sources, as for the wave paths sketched in the top panel of Figure 8. To evaluate these unwanted

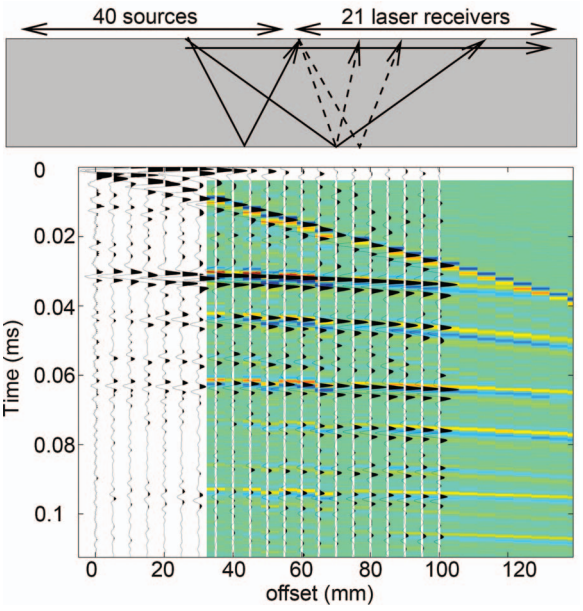

Figure 7. Top: Experimental geometry with 21 receivers recorded for 40 sources. The solid lines are some of the wave paths for one shot record. The dashed lines are wave paths for a virtual source. Bottom: One shot record (color online) overlain by 21 receivers crosscorrelated with the first receiver (wiggles).

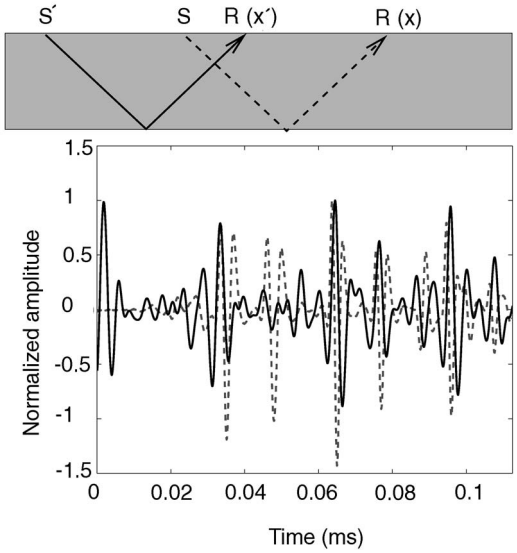

Figure 8. Bottom: Comparison between $\dot{\underline{D}}(t)$ (solid line) and $\tilde{G}(x', x, t)$ (dashed line, same as in Figure 1). The correlation between the two wavefields is 0.28 (top panel).

correlations, the wavefields first are summed over all sources, effectively setting off all 40 sources at once. Then the derivative of the crosscorrelation is calculated:

$$\dot{\underline{D}}(t) = \frac{d}{dt}\left(\sum_{s=1}^{N} \tilde{G}(x^s, x, t) \star \sum_{s'=1}^{N} \tilde{G}(x^{s'}, x', t) \right). \quad (6)$$

This way, there are terms in $\dot{\underline{D}}(t)$ when $s \neq s'$, such as wave paths drawn in the top of Figure 8. These are generally called *crossterms* or *interference terms*. These are waves that do not cross both receivers. Hence, these peaks in the crosscorrelation do not relate to the Green's function between receivers.

The bottom panel of Figure 8 compares the direct measurement $\tilde{G}(x', x, t)$ to $\dot{\underline{D}}(t)$. In these experiments, the sources are correlated, because it is, in principle, the same source function $S(t)$ at a different location. Only small variations in the physical coupling between source and granite slab might uncorrelate the individual source functions. Completely uncorrelated sources would not amplify this mismatch between $\tilde{G}(x', x, t)$ and $\dot{\underline{D}}(t)$, but in this case their correlation factor is 0.28. The strong correlation in $\dot{\underline{D}}(t)$ near the origin implies that equidistant wave paths from correlated sources, as drawn in the top panel of Figure 8, indeed exist. One could consider this the worst case scenario of strongly correlated sources, but field studies might observe strong correlation as well in seismic sources from water waves crashing on shore, or microseismic activity.

DISCUSSION AND CONCLUSIONS

Seismology may have taken up a completely new way of imaging the earth's interior by crosscorrelating signals recorded at different receiver locations. However, to obtain the full Green's function, equipartition of energy is needed. This means that we would need either strong scattering (and little intrinsic absorption), or sources distributed everywhere throughout the medium. Nevertheless, controlled ultrasonic experiments, with only a limited number of sources in a small region on the surface, show robust estimates of the

vertical component of the particle acceleration impulse response. For such an estimate of the impulse response, actual waves, that pass through both receivers, are needed. This signal may be weak and/or of unknown origin, but should not be considered ambient or incoherent noise. When the responses of these sources overlap in the recording time, correlation between the sources dramatically diminish the quality of the estimated Green's function between receivers.

Perhaps one can imagine the multitude of different ray paths and wave modes in a 3D elastic experiment, leading to correlations in the recorded wavefields. In 2D examples and acoustics or 3D examples dominated by surface waves, the number of possible wave paths is smaller, leading to striking estimates of the impulse response via crosscorrelation. The accuracy of the estimate of the Green's function lies in a choice of source positions, so that the crosscorrelated waveforms include the points of stationary phase. In this case, sources were limited to one side of the receivers, recovering only a one-sided Green's function.

ACKNOWLEDGMENTS

This work is supported by the National Science Foundation (EAR-0337379) and the Army Research Office (DAAD19-03-1-0292). I thank John Scales, Matt Haney, Karim Sabra, Rodney Calvert, Justin Hedley, Andreas Rüger, Ludmila Adam, Deyan Draganov, and Kees Wapenaar for many useful discussions.

REFERENCES

Bakulin, A., and R. Calvert, 2004, Virtual source: new method for imaging and 4D below complex overburden: 74th Annual International Meeting, SEG, Expanded Abstracts, 2477–2480.

Campillo, M., and A. Paul, 2003, Long-range correlations in the diffuse seismic coda: Science, **299**, 547–549.

Derode, A., E. Larose, M. Tanter, J. de Rosny, A. Tourin, M. Campillo, and M. Fink, 2003, Recovering the Green's function from field-field correlations in an open scattering medium (l): Journal of the Acoustical Society of America, **113**, 2973–2976.

Duvall, T. L., S. M. Jeffferies, J. W. Harvey, and M. A. Pomerantz, 1993, Time/distance helioseismology: Nature, **362**, 430.

Lee, Y. W., 1960, Statistical theory of communication: John Wiley.

Lobkis, O. I., and R. L. Weaver, 2001, On the emergence of the Green's function in the correlations of a diffuse field: Journal of the Acoustical Society of America, **110**, 3011–3017.

Malcolm, A. E., J. A. Scales, and B. A. van Tiggelen, 2004, Extracting the Green function from diffuse, equipartitioned waves: Physical Review E, **70**, 015601.

Nishizawa, O., T. Satoh, X. Lei, and Y. Kuwahara, 1997, Laboratory studies of seismic wave propagation in inhomogeneous media using a laser Doppler vibrometer: Bulletin of the Seismology Society of America, **87**, 809–823.

Rickett, J. E., and J. F. Claerbout, 1999, Acoustic daylight imaging via spectral factorization; helioseismology and reservoir monotoring: The Leading Edge, **18**, 957–960.

Roux, P., K. G. Sabra, W. A. Kuperman, and A. Roux, 2005, Ambient noise cross correlation in free space: Theoretical approach: Journal of the Acoustical Society of America, **117**, 79–84.

Sabra, K. G., P. Gerstoft, P. Roux, W. A. Kuperman, and M. C. Fehler, 2005, Surface wave tomography from microseisms in Southern California: Geophysical Research Letters, **32**, L14311–L14311.

Scales, J. A., and K. van Wijk, 1999, Multiple scattering attenuation and anisotropy of ultrasonic surface waves: Applied Physics Letters, **74**, 3899–3901.

Schuster, G. T., J. Yu, J. Sheng, and J. Rickett, 2004, Interferometric/daylight imaging: Geophysical Journal International, **157**, 838–853.

Shapiro, N. M., and M. Campillo, 2004, Emergence of broadband Rayleigh waves from correlations of the ambient seismic noise: Geophysical Research Letters, **31**, L07614.

Shapiro, N. M., M. Campillo, L. Stehly, and M. H. Ritzwoller, 2005, High-resolution surface-wave tomography from ambient seismic noise: Science, **307**, 1615–1618.

Snieder, R., 2004, Extracting the Green's function from the correlation of coda waves: A derivation based on stationary phase: Physical Review E (Statistical, Nonlinear, and Soft Matter Physics), **69**, 046610.

Wapenaar, K., 2004, Retrieving the elastodynamic Green's function of an arbitrary inhomogeneous medium by cross correlation: Physical Review Letters, **93**, 254301.

Wapenaar, C. P. A., and J. Fokkema, 2006, Green's function representations for seismic interferometry, (this issue).

Weaver, R. L., and O. I. Lobkis, 2001, Ultrasonics without a source: Thermal fluctuation correlations at MHz frequencies: Physical Review Letters, **87**, 134301.